GeoStorage

Vol. 1, No. 1, p. 42-55, 2025

Original article

Two-phase Seepage Pore Pressure Diffusion Wave-saturation Model and Its Application in CO_2 Geological Storage

Min Hao[1,2], Bing Bai[1]*, Lu Shi[1], Hongwu Lei[1], Hengtao Yang[1], Duoxing Yang[3]

[1] *State Key Laboratory of Geomechanics and Geotechnical Engineering Safety, Institute of Rock and Soil Mechanics, Chinese Academy of Sciences, Wuhan 430071, China*
[2] *University of Chinese Academy of Sciences, Beijing 100049, China*
[3] *National Institute of Natural Hazards, Ministry of Emergency Management of China, Beijing 100085, China*

Keywords:
Pore pressure diffusion wave
two-phase seepage
analytical solution of saturation
CO_2 geological storage
leakage risk assessment

Cited as:
Hao m, Bai B, Shi L, et al. 2025. Two-phase Seepage Pore Pressure Diffusion Wave-saturation Model and Its Application in CO_2 Geological Storage. *GeoStorage*, 1(1), 42-55.
https://doi.org/10.46690/gs.2025.01.03

Abstract:
This study developed a one-dimensional coupled model of two-phase seepage and pore pressure diffusion wave-saturation interaction based on the theory of pore pressure diffusion waves. Analytical solutions for fluid saturation distribution and the leading edge position were derived, and the interaction mechanism between pore pressure and saturation fields was systematically analyzed. The study revealed the governing law of the coupling effects between pressure diffusion waves and two-phase seepage on fluid migration: in the short term, the process was dominated by pressure-driven rapid migration, while in the long term, it approached a stable diffusion equilibrium. Through a parameter sensitivity analysis, the critical influences of the diffusion coefficient and pore pressure on the advancement of the migration front were clarified, and the model's applicability to CO_2 geological storage was explored. The results indicate that dynamic sealing in heterogeneous reservoirs and high permeability zones can enhance storage efficiency through a stepped injection pressure strategy. Additionally, the proposed leakage grading evaluation method offers a theoretical foundation for engineering risk management and control. This study provides a novel conceptual framework and analytical tool to ensure long-term safety and optimize the design of CO_2 storage projects.

1 Introduction

The study of fluid dynamics in porous media has broad applications in fields such as oil and gas recovery, environmental remediation and carbon dioxide (CO_2) geological storage (Blunt and Lin, 2022; Yang et al., 2014). In global carbon neutrality, geological carbon storage (GCS) has gained considerable attention due to its substantial potential to reduce greenhouse gas emissions (Abanades et al., 2005). A central scientific challenge in GCS is accurately predicting the long-term migration and storage stability of injected CO_2 within subsurface formations. The theory of pore pressure diffusion waves offers a novel approach to address this challenge by accounting for the dynamic propagation of pressure signals through porous media (Mandelis, 1991, 2001; Silin et al., 2003). This theory captures the essence of dynamic pressure diffusion by incorporating the effects of fluid compressibility and medium permeability (Norris 1993), and in partially saturated porous media, the dynamic response of pore pressure is also significantly affected by multiphase flow characteristics such as fluid saturation distribution and capillary pressure change (Zhang and Ping, 2022).

Recent studies have shown that pore pressure diffusion waves play a critical role in a variety of geophysical phenomena, including microseismicity induced by underground fluid injection (Sminchak and Gupta 2003; Lei et al. 2008; Keranen et al. 2014), hydraulic fracturing in shale gas development (Rasouli and Sutherland, 2014), viscous fingering triggered by pressure fluctuations during CO_2 injection (Yang et al. 2011),

Yandy Scientific Press

* Corresponding author.
E-mail address: 2951437199@qq.com (Hao m); bbai@whrsm.ac.cn (Bai B); lshi@whrsm.ac.cn (Shi L); hwlei@whrsm.ac.cn (Lei HW); htyang@mail.whrsm.ac.cn (Yang HT); dxyangcea@yahoo.com (Yang DX)

Received Jul. 18, 2025; revised Aug. 19, 2025; accepted Sep. 1, 2025; available online Sep. 7, 2025.

Zhang and Ping by extending Biot's theory, derived an explicit fundamental solution for pore pressure induced by a fluid mass source in partially saturated porous media (Zhang and Ping, 2022). They found that pore pressure disturbances can propagate either as oscillatory waves or exhibit static diffusion, and that the coexistence of these two physical processes is closely related to the fluid injection rate and the characteristic frequency of the medium. This research provides key theoretical support for understanding micro-seismic activity triggered by subsurface fluid injection, indicating that the coupling between pressure diffusion and wave processes may directly affect reservoir stability. Furthermore, Abdullahi et al. observed in their study on enhanced oil recovery using elastic wave stimulation that the amplitude of the pore pressure gradient in partially saturated reservoirs is significantly higher than that in fully saturated reservoirs under low-frequency (3 Hz) seismic stress (Abdullahi et al., 2024). They attributed this difference to the regulatory effect of capillary pressure on cross-layer fluid flow and ground deformation in saline aquifers which further confirms the uniqueness of pore pressure dynamic responses in multiphase flow environments (Li et al., 2014; Lei et al., 2011). . Investigating these waves enhances our understanding of the underlying physical mechanisms and supports risk assessment and leakage analysis in CO_2 storage projects (Mandelis, 2001).

Despite its significance, conventional two-phase seepage models- such as the Buckley-Leverett equation-typically assume steady-state or quasi-steady-state flow, neglecting the non-equilibrium effects induced by pore pressure diffusion (Leverett and Lewis, 1941). These models simplify saturation distributions as functions of relative permeability and Darcy velocity, limiting their applicability to scenarios involving dynamic pressure propagation (Nordbotten and Celia, 2011). Kenzhebek et al. pointed out that standard numerical methods for the Buckley-Leverett model (such as finite difference and finite volume schemes) often suffer from numerical dispersion issues (Kenzhebek et al., 2025). Although Physics-Informed Neural Networks (PINNs) offer a new approach for solving multiphase flow equations, they still require the introduction of artificial diffusion terms to capture sharp saturation fronts while balancing computational stability and physical accuracy. This challenge fundamentally stems from the theoretical gap in understanding the dynamic coupling mechanism between the pressure field and the saturation field.

Current research on fluid migration in porous media generally follows two paths: numerical modeling based on Darcy's law and the continuity equation (Garcia and Silveira, 2024; DiCarlo, 2004; Wang et al., 2021a), and analytical modeling of pressure diffusion waves for single-phase flow (Yang et al., 2015; Thomsen, 1995). While numerical simulations accommodate heterogeneity and complex boundary conditions, they are computationally intensive and sensitive to meshing strategies. Analytical methods are more efficient but are often restricted to single-phase flow, leading to the decoupling of pressure and saturation fields. This decoupling may be tolerable for short-term analyzes but undermines model reliability in long-term CO_2 storage assessments, which span decades to centuries (Pruess et al., 1999).

Recent efforts have aimed to incorporate dynamic pressure effects into multiphase flow models (Jha and Juanes, 2007; Kim et al., 2011; Lu and Wheeler, 2020). For example, (Zhang et al., 2020) developed a three-dimensional pore-network model for multiphase flow that captures non-wetting phase migration but does not account for pressure–saturation coupling. Yang et al. investigated pore pressure wave propagation in saturated and dual-porosity media, focusing exclusively on single-phase systems (Yang et al., 2015, 2016). Full-wavefield simulations based on Biot's theory (Zhang, 2014) suggested interactions between pore pressure and saturation but lacked analytical solutions. Additionally, core-scale experiments (Zhang et al., 2024) and reservoir studies (Li et al., 2008; Wang et al., 2021a) have identified features such as initial pressure gradients and gas - water interactions. Nwankwo et al. found that shale's ultra-low permeability (nano- to micro-darcy) and strong anisotropy significantly alter the pressure diffusion coefficient, impacting CO_2 storage efficiency. This underscores the need for research on pressure diffusion-multiphase flow coupling in shale and CO_2 sequestration contexts (Nwankwo et al., 2025). These limitations highlight three key gaps in current research:

(1) Most existing models fail to adequately account for the bidirectional coupling between the pressure and saturation fields. For instance, although Zhang and Ping developed a model describing the transition between pressure waves and diffusion in partially saturated media, their work did not incorporate practical multiphase systems such as CO_2-brine (Zhang and Ping, 2022);

(2) The absence of analytical solutions with clear physical interpretations remains a significant challenge. Although the Physics-Informed Neural Network (PINN) model developed by Kenzhebek et al. can simultaneously predict pressure and saturation, it remains largely data-driven and exhibits limited physical interpretability (Kenzhebek et al., 2025);

(3) There is insufficient validation of their applicability to specific scenarios such as CO_2 geological storage. Although the study by Abdullahi et al. addressed pore pressure responses in partially saturated reservoirs (Abdullahi et al., 2024), it did not specifically analyze the unique processes occurring during CO_2 injection, such as gas dissolution and changes in interfacial tension. Addressing these gaps is crucial for both theoretical advancement and practical application.

This study develops a one-dimensional coupled model that integrates the analytical solution for pressure diffusion waves in saturated porous media (Yang et al., 2016) with a two-phase flow framework. The model investigates the roles of the diffusion coefficient and pore pressure in controlling fluid migration and migration front advancement and evaluates its applicability to CO_2 geological storage. Furthermore, the study elucidates a self-regulation mechanism in which pressure diffusion waves mitigate leakage behavior, offering theoretical support for optimized storage design. These findings not only extend the theoretical understanding of fluid migration i n porous media but also provide a robust analytical tool for engineering applications.

2 Model and solution

2.1 Pore pressure diffusion wave–saturation model of two-phase seepage

Yang et al integrated the classical diffusion equation proposed by Silin and Korneev(Silin et al., 2003) (Eq. 1) with the initial and boundary conditions specified in Eq.2 (Yang et al., 2016). Through a series of analytical derivations, they obtained a closed-form solution Eq. 3 describing the propagation of pore pressure diffusion waves in a one-dimensional, semi-infinite, homogeneous porous medium. The solution is expressed in terms of the error function (erf), which captures the transient behavior of pressure diffusion over time and space.

$$\frac{\partial P(x,t)}{\partial t} = D\frac{\partial^2 P(x,t)}{\partial x^2} \tag{1}$$

where $P(x,t)$ is the pore pressure (Pa), D is the pressure diffusion coefficient, which is defined as: $D = \frac{k}{\varphi\beta c}$ where k is the permeability of porous media [mD], φ is the porosity (%), β is the compression coefficient (1/Pa), and μ is the fluid viscosity (Pa·s).

$$\begin{aligned} &t = 0, \quad x > 0, \quad P = P_0, \\ &t > 0, \quad x = 0, \quad P(0,t) = P_1, \\ &t > 0, \quad x = \infty, \quad P(\infty,t) = P_0. \end{aligned} \tag{2}$$

where P_0 is the initial pore pressure, P_1 is the inlet injection pressure.

$$P(x,t) = P_1 + (P_0 - P_1)erf(\frac{x}{2\sqrt{Dt}}) \tag{3}$$

The gradient of the analytical pressure solution in the x-direction is given by:

$$\frac{\partial P(x,t)}{\partial x} = \frac{P_0 - P_1}{\sqrt{\pi Dt}} e^{-\frac{x^2}{4Dt}} \tag{4}$$

The analytical solution of the pore pressure diffusion wave reveals that its propagation is primarily governed by diffusion mechanisms, with its velocity and attenuation characteristics strongly dependent on key properties such as permeability, porosity, and fluid viscosity. As the frequency increases, the diffusion wave propagates faster; however, it also undergoes greater attenuation, demonstrating a pronounced frequency-dependent behavior. At low frequencies, this results in substantial attenuation, where diffusion dominates-particularly under low-frequency pressure perturbations (Mandelis and Hess, 1997).

2.1.1 Basic assumptions

The two-phase flow model serves as a mathematical framework for investigating the simultaneous movement of two immiscible fluids in porous media. At its core, the model describes the dynamic distribution, flow, and interaction of the two fluids, as governed by mass conservation equations and Darcy's law. When extending the single-phase pore pressure diffusion wave theory to two-phase flow, it is essential to clearly define the model's fundamental assumptions and boundary conditions. The present model is developed under the following assumptions:

(1) Incompressible fluids: both fluids are assumed to be incompressible, implying that their densities remain constant under pressure variations;

(2) Negligible capillary, interfacial, and gravitational effects: Capillary pressure, interfacial tension, wettability, and gravity are not explicitly considered.These forces are considered negligible in simplified models, particularly under low-flow or homogeneous conditions. This simplification facilitates analytical derivation, but it should be noted that in real multiphase systems, these interfacial parameters significantly influence flow behavior by governing P_c-S_w (capillary pressure–saturation) and K_r-S_w (relative permeability–saturation) relationships;

(3) Homogeneous porous medium: Permeability, porosity, and other properties are assumed to be spatially uniform;

(4) Steady-state relative permeability: Relative permeability is considered a function of saturation that remains constant over time.

These assumptions simplify the system and make it possible to derive closed-form analytical solutions. In practice, neglecting gravity and capillary forces can be reasonable under low-flow or homogeneous conditions, although such effects become more pronounced in high-flow regimes or heterogeneous media (Leverett and Lewis, 1941). Nevertheless, interfacial parameters such as interfacial tension σ and wettability θ play critical roles in controlling capillary pressure and shaping relative permeability–saturation relationships. Excluding these effects inevitably limits the model's physical completeness, and future work should incorporate calibrated Pc-Sw and K_r-S_w curves to better capture the complexity of CO_2–water–rock interactions in geological formations.

2.1.2 Governing equation

The governing equations of the two-phase seepage model consist of the continuity equation and the momentum equation. For each fluid, the continuity equation represents mass conservation, while the momentum equation characterizes the flow behavior, typically governed by Darcy's law.

Continuity equation:

$$\varphi\frac{\partial S_i'(x,t)}{\partial t} + \frac{\partial V_i}{\partial x} = 0 \tag{5}$$

Momentum equation:

$$V_i = -\frac{KK_{ri}}{\mu_i}\frac{\partial P(x,t)}{\partial x} \tag{6}$$

where S_i is the fluid saturation; K_ri is the relative permeability of fluid.

2.2 Solution of saturation

The interaction between pore pressure diffusion waves and two-phase flow involves bidirectional coupling: pore pressure variations alter fluid saturation distribution, while fluid flow feedback affects the pressure field. Under the assumptions of negligible capillary forces and gravity and a non-zero initial

pressure, the saturation coupling equation is derived by combining Eq. 4 with Eqs. 5 and 6:

$$\frac{\partial S_i(x,t)}{\partial t} + \frac{1}{\varphi}\frac{\partial}{\partial x}\left[-\frac{KK_{ri}}{\mu_i}\frac{P_0 - P_1}{\sqrt{\pi Dt}}e^{\frac{-x^2}{4Dt}}\right] = 0 \tag{7}$$

The general solution of saturation, obtained by simplifying and solving the partial differential equation, is given as:

$$S_i(x,t) = -\frac{\sqrt{D}KK_{ri}(P_1 - P_0)Erf[\frac{x}{2\sqrt{Dt}}]}{D\mu_i\varphi} + C_1 \tag{8}$$

where C_i is an integration constant. The analytical solution for saturation can be fully determined by specifying appropriate initial and boundary conditions.

This coupling mechanism illustrates the mutual interaction between the pore pressure diffusion wave and two-phase seepage. Changes in pore pressure drive fluid flow and saturation redistribution, while variations in fluid saturation, in turn, alter the pressure distribution.

Based on the general solution of saturation in Eq. 8, it is assumed that the saturation distribution of the injected fluid satisfies the following initial and boundary conditions:

$$\begin{aligned} t = 0, x > 0, S_i = S_k \\ t > 0, x = 0, S_i(0,t) = S_{im} \\ t > 0, x = \infty, S_i(\infty,t) = S_k. \end{aligned} \tag{9}$$

where $S_{im}$is the maximum saturation of the fluid and S_{ic} is the irreducible (bound) saturation.

By substituting these conditions into Eq. 8, the analytical solution for saturation becomes:

$$S_i(x,t) = S_{im} - (S_{im} - S_{ic})erf[\frac{x}{2\sqrt{Dt}}] \tag{10}$$

This solution satisfies the specified initial and boundary conditions. It is worth noting that both the maximum and irreducible saturations are influenced by the initial pressure distribution of the formation, with the pressure effect implicitly embedded in the derivation of Eq. 10. This analytical solution describes the propagation of the saturation front within the porous medium. In reservoir engineering, this saturation front can characterize waterfront advancement during water flooding or the migration of the CO_2 plume during CO_2 injection.

2.3 Leading edge of saturation

The leading edge advance equation of saturation (also known as the leading edge velocity equation) describes the progression of the fluid saturation front-specifically, the position where the saturation decreases from a higher to a lower value-within porous media over time.

The leading edge refers to the position where the saturation transitions from S_{im} to S_{ic}. A specific saturation value S_f is defined as the leading edge threshold. Suppose $S_f = S_{im} - \varepsilon(S_{im} - S_{ic})$, where is a decimal number close to 0, indicating the position at which saturation approaches S_{ic}.

By substituting $S_i(x,t) = S_f$ into the saturation analytical solution in Eq. 10, we obtain:

$$S_f = S_{im} - (S_{im} - S_{ic})erf[\frac{x_f}{2\sqrt{Dt}}] \tag{11}$$

By solving the leading edge position x_f we obtain:

$$x_f = 2\sqrt{Dt}\mathrm{erf}^{-1}(\varepsilon) \tag{12}$$

where $erf^{-1}(\varepsilon)$ is the value of the inverse function of the error function at ε.

The leading edge velocity v_f is the derivative of the leading-edge position x_f concerning time t , expressed as:

$$v_f = \frac{dx_f}{dt} = \frac{\sqrt{D}erf^{-1}(\varepsilon)}{\sqrt{t}} \tag{13}$$

The above analytical results provide a theoretical foundation for investigating the migration characteristics of CO_2 in porous media. To verify the model's reliability and explore the influence of various parameters on the migration process, system verification, and parameter sensitivity analyses will be conducted through numerical examples.

3 Model validation and parameter sensitivity analysis

In this section, the fluid migration characteristics of CO_2 injected into saturated porous media in a one-dimensional, semi-infinite space are analyzed through specific examples. The parameters used in the analysis are provided in Table 1. First, the validity of the analytical solution is verified through a simulation analysis of short-term, short-distance injection. Subsequently, the long-term, long-distance migration characteristics and the sensitivity of key parameters are analyzed in detail.

3.1 Comparative analysis of analytical solution and numerical solution

To verify the model's accuracy, the saturation distribution under short-term injection was simulated and analyzed. Fig.1 compares the saturation distribution curves obtained from both the analytical and numerical solutions at various time intervals (30, 60, and 90 seconds). At all the time points, the results from both solutions demonstrate strong agreement in the overall trend of saturation distribution. Although the saturation curve from the numerical solution shows a steeper decline in regions farther from the injection point, the analytical solution demonstrates a more gradual attenuation. This discrepancy may arise from discretization errors in the numerical method (e.g., grid division, time step selection) or the approximate simplifications of the boundary conditions. Nevertheless, the numerical solution closely follows the overall evolution predicted by the analytical solution, confirming the theoretical robustness of the model.

From the diagram, it is evident that in the short-term, short-range scenario, as time progresses (from 30 seconds to 90 seconds), the downward trend of the saturation curve becomes

Tab. 1 Comparison of Several Typical Underground Granaries

$P_1 - P_0$ (Pa)	S_{im}	S_{ic}	φ (%)	K_{m^2}	K_{ri}	β (Pa^{-1})	μ_i (Pa·s)
2.32×10^{10}	0.95	0.05	0.02	1×10^{-18}	0.3	1×10^{-9}	3×10^{-5}

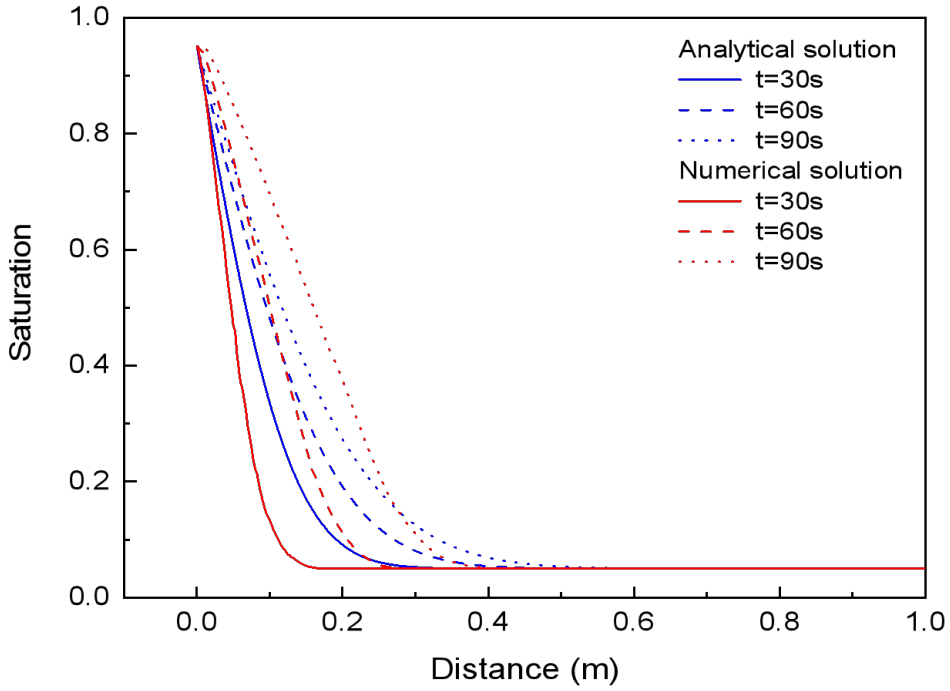

Fig. 1 Comparison of the analytical and numerical solutions for short-term injection

more gradual and eventually levels off (with the maximum migration distance not exceeding 0.8 meters). This suggests that the fluid front's advancing speed decreases over time. During the initial injection phase, the fluid rapidly diffuses and occupies the area near the injection point. The saturation front advances quickly, and the saturation decreases sharply. Over time, the diffusion effect within the porous medium smooths the saturation curve, and the saturation change stabilizes, indicating that the fluid front's advancement reaches a dynamic equilibrium. At this point, fluid migration effectively ceases. From a dynamic perspective, the steep saturation drop in the initial stage reflects the rapid advancement of the fluid front, driven primarily by the injection pressure. The gradual attenuation of the saturation distribution suggests that the resistance of the porous media and the fluid diffusion effect become increasingly dominant, leading to a reduction in the leading edge's propulsion speed and reaching dynamic equilibrium. This phenomenon highlights the coupling mechanism between the pressure diffusion wave and two-phase seepage: the dynamic attenuation of pore pressure indirectly inhibits the continuous expansion of the leading edge by modulating the saturation gradient.

The results in Fig.1 demonstrate that both the analytical and numerical solutions show good consistency in predicting saturation distribution at various time points. As time progresses, the fluid front's advancing speed slows down, and the saturation distribution stabilizes. These findings are crucial for understanding the short-term dynamic behavior of fluid migration in porous media, especially in engineering applications involving rapid fluid injection.

3.2 Analysis of long-distance migration characteristics of fluid saturation

Fig.2 illustrates the dynamic evolution of CO_2 fluid saturation as a function of distance over various time scales (60 seconds, 1 day, 1 month, 6 months, 1 year, and 2 years) under long-term and long-distance migration conditions. During the initial injection stage (t = 60 seconds), the fluid exhibits strong pressure-driven behavior, and the saturation curve displays a sharp decline from nearly 1 to approximately 0, indicating that the pressure diffusion wave dominates the migration dynamics at this early stage. By 1 month, the migration front advances to approximately 200 m, but the saturation gradient becomes significantly attenuated, suggesting that diffusive transport begins to dominate the migration process. Notably, between 6 months and 2 years, the migration front gradually progresses to approximately 600 m. At this stage, the saturation curve becomes nearly flat, and the saturation at 600 m stabilizes below 0.01, indicating that the CO_2 migration has reached a dynamic equilibrium.

This evolution pattern reveals three key characteristics:

(1) The influence of pressure-driven flow is primarily limited to the initial 200 m within the first month;

(2) 600 m can be regarded as the effective safe storage boundary under the given conditions;

(3) A 2-year period is sufficient for the system to reach a

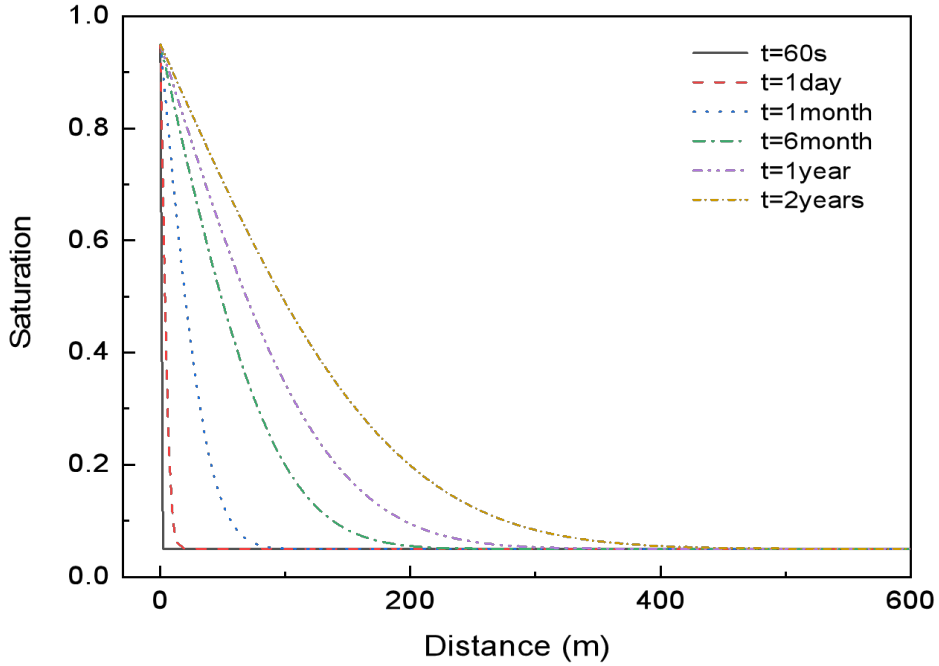

Fig. 2 Temporal evolution of fluid saturation at various time intervals

stable state. These findings provide a crucial basis for site selection and risk assessment of large-scale CO_2 storage projects, particularly highlighting that natural diffusive processes can effectively ensure storage safety over appropriate time scales.

The results presented in Fig.2 indicate that both the fluid saturation distribution and the velocity of the advancing front vary significantly over time. In the early stage, the fluid rapidly diffuses and saturates the proximal region, whereas in the long term, the diffusion rate decreases and the saturation distribution gradually stabilizes.

3.3 Analysis of dynamic characteristics of leading-edge propagation

Fig.3 quantitatively illustrates the time evolution of the leading-edge advancement distance (x_f) and velocity (v_f). At the early stage, the leading edge exhibits typical pressure-driven behavior: the advancement distance increases linearly, and the corresponding v_f remains high, reflecting a strong displacement effect dominated by injection pressure, with the fluid front diffusing rapidly through the porous medium. As time progresses (100–15,000 s), the system exhibits a distinct transition: the growth of x_f follows a $\sqrt{t}$ dependence, and v_f decreases rapidly to below 4×10^{-4}m/s, indicating that the advancement of the fluid front nearly ceases, and the system gradually approaches a dynamic equilibrium. The entire process can be divided into three stages: (1) an initial rapid advancement stage dominated by pressure wave propagation; (2) a transition stage characterized by the balance between diffusion and resistance; (3) a long-term equilibrium stage governed by seepage–diffusion coupling.

The results presented in Fig. 3 demonstrate that both the advancement distance and velocity of the fluid front vary significantly over time. Initially, the fluid front advances rapidly; however, over time, the propulsion velocity decreases and eventually approaches a steady state.

3.4 Effect of diffusion coefficient on saturation distribution and leading edge advancement

Fig.4 illustrates the regulatory effect of different diffusion coefficients ($D, 2D, 4D$) on fluid migration behavior. At a fixed time scale (t = 1 year), an increase in the diffusion coefficient significantly alters the saturation distribution. In all cases, saturation decreases with increasing distance, although the decay rate varies depending on the diffusion coefficient. A lower diffusion coefficient (D) results in a rapid drop in saturation over a short distance, whereas a higher diffusion coefficient ($4D$) sustains elevated saturation levels over a longer range. When the diffusion coefficient is increased from the baseline value to $4D$, the characteristic length scale of the saturation profile extends from approximately 200 m to 600 m, and the saturation gradient within the proximal region (0–100 m) decreases from $-0.0061\ m^{-1}$ to $-0.003\ m^{-1}$. This observation indicates that a higher diffusion coefficient promotes a more uniform fluid distribution, resulting in a smoother and more gradual advancement of the leading edge.

From an engineering perspective, these results imply that:

(1) accurate determination of the diffusion coefficient is critical for predicting the storage extent, as errors in D can lead to a $\sqrt{D}$ deviation in the estimated position of the leading edge;

(2)Artificial manipulation of reservoir parameters (e.g., increasing porosity φ or reducing fluid viscosity μ) to enhance the effective diffusion coefficient can significantly improve CO_2 spatial distribution control. These findings provide a quantitative foundation for storage site selection and engineering design.

Fig.5 shows the time-dependent evolution of the leading edge position under different diffusion coefficients ($D, 2D, 4D$). The

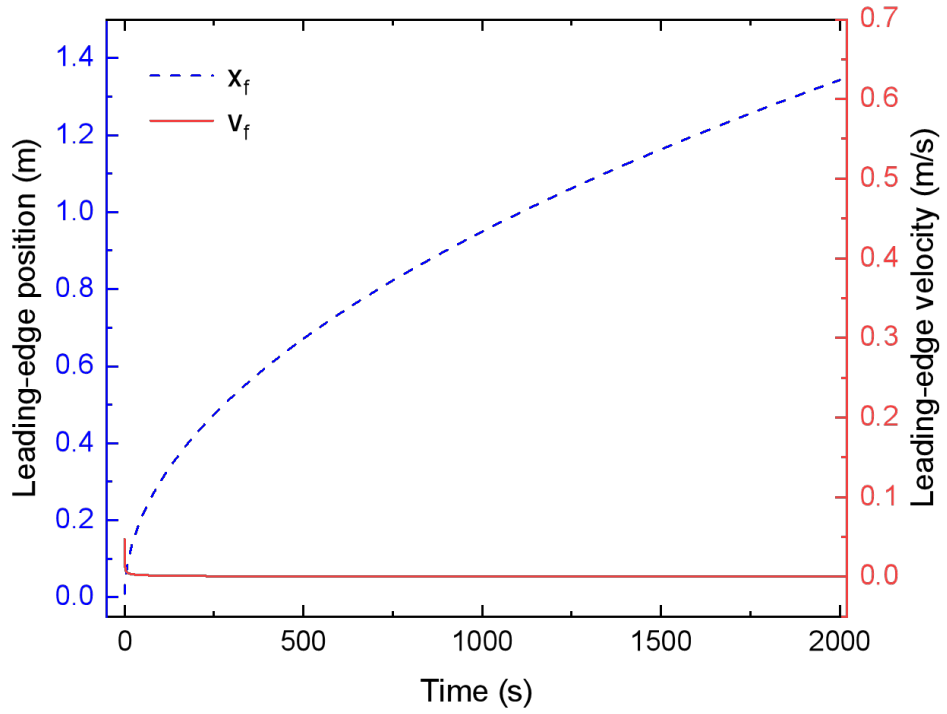

Fig. 3 Time-dependent evolution of leading-edge advancement distance and velocity

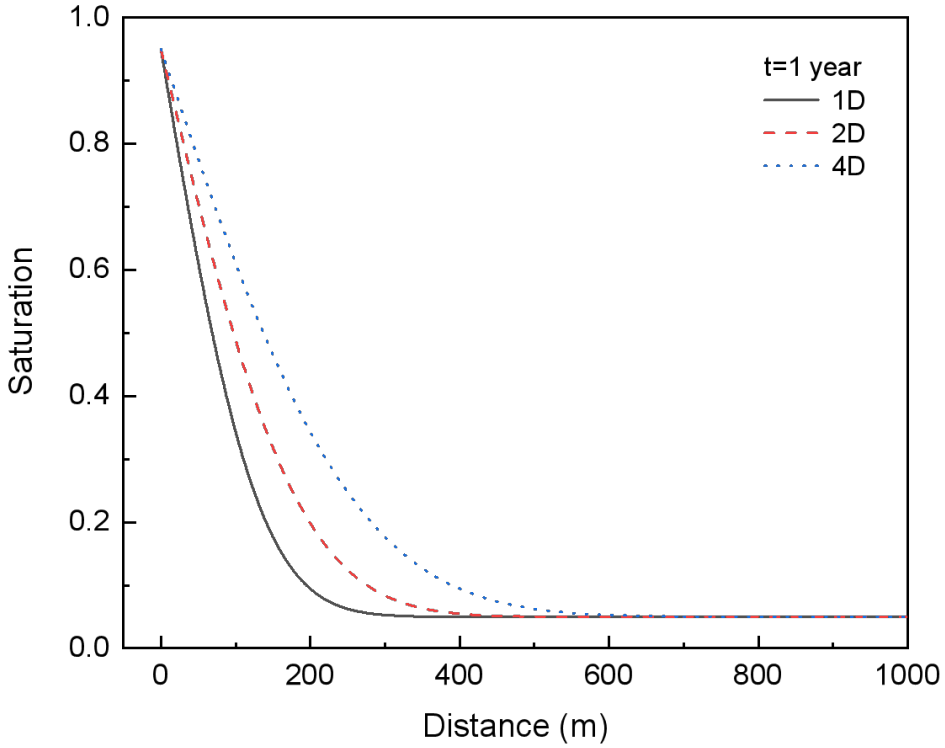

Fig. 4 Saturation versus distance curves under different diffusion coefficients (t = 1 year)

diffusion coefficient significantly influences the leading edge position. As the diffusion coefficient increases, the advancement of the leading edge accelerates. This indicates that a higher diffusion coefficient enhances fluid migration in the porous medium, resulting in faster advancement of the leading edge.

In all cases, the leading edge position increases over time, although the rate of increase varies depending on the diffusion coefficient. A lower diffusion coefficient (D) results in a slower progression of the front, while a higher coefficient ($4D$) yields a faster advance. This difference reflects the direct influence of

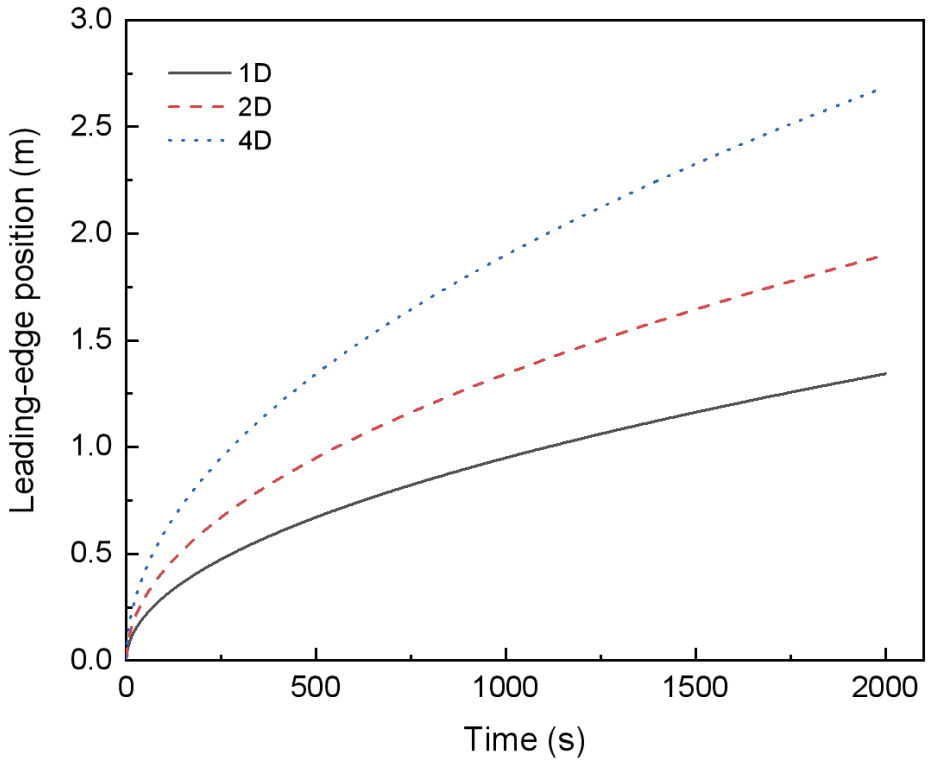

Fig. 5 Temporal evolution of the leading edge position under different diffusion coefficients ($D, 2D, 4D$)

the diffusion coefficient on fluid migration dynamics.

At longer times (beyond 2000 seconds), the predicted leading-edge positions continue to increase, although the rate of increase gradually slows. This suggests that, over time, the dynamic driving force of fluid migration weakens, resulting in a slower advancement of the leading edge.

Fig.6 shows the evolution of the leading-edge velocity over time under different diffusion coefficients ($D, 2D, 4D$). At the initial moment (near 0 seconds), the leading-edge velocity in all cases decreases rapidly and then stabilizes. This indicates that during the early stage of fluid injection, the leading-edge undergoes a rapid deceleration. The curve corresponding to the highest diffusion coefficient exhibits the greatest initial velocity, whereas the curve with the lowest diffusion coefficient shows the smallest initial velocity. This reflects enhanced fluid migration associated with higher diffusion coefficients.

After the initial deceleration, the leading edge velocity quickly stabilizes at a very low value, approaching 0 m/s. This suggests that during the later stage of migration, the front velocity becomes negligible, indicating near cessation of movement. This stable condition may result from the establishment of hydrodynamic equilibrium or from limitations imposed by the permeability of the porous medium.

Throughout the observation period, the velocity associated with the $4D$ case remains higher than those of the $2D$ and D cases. This indicates that a higher diffusion coefficient helps sustain a greater migration front velocity. However, over time, the differences in leading edge velocity among different diffusion coefficients diminish and eventually converge to a common stable value.

The results in Fig.6 demonstrate that the diffusion coefficient has a significant impact on the prediction of migration front velocity, particularly during the early stage. A higher diffusion coefficient results in faster initial front velocity; however, in the long term, velocities under all conditions converge to a similar stable value.

4 Applications and discussions

The two-phase seepage pore pressure diffusion wave–saturation model developed in the preceding sections serves as a quantitative framework to analyze critical challenges in CO_2 geological storage engineering. This section focuses on the complex geological conditions of real-world reservoirs, such as heterogeneity and high-permeability zones, and explores the model's performance characteristics and control strategies within practical engineering scenarios. It further elucidates the dual effects of geological heterogeneity on both storage efficiency and long-term safety, providing a scientific foundation for site selection and the optimization of site-specific injection strategies.

4.1 Dynamic sealing mechanism in heterogeneous reservoirs and high-permeability zones

4.1.1 Influence of reservoir heterogeneity on sealing behavior

Fig.7 illustrates the critical role of reservoir heterogeneity in controlling fluid migration by comparing the evolution of fluid saturation profiles with distance in homogeneous and heterogeneous formations. Under homogeneous reservoir conditions

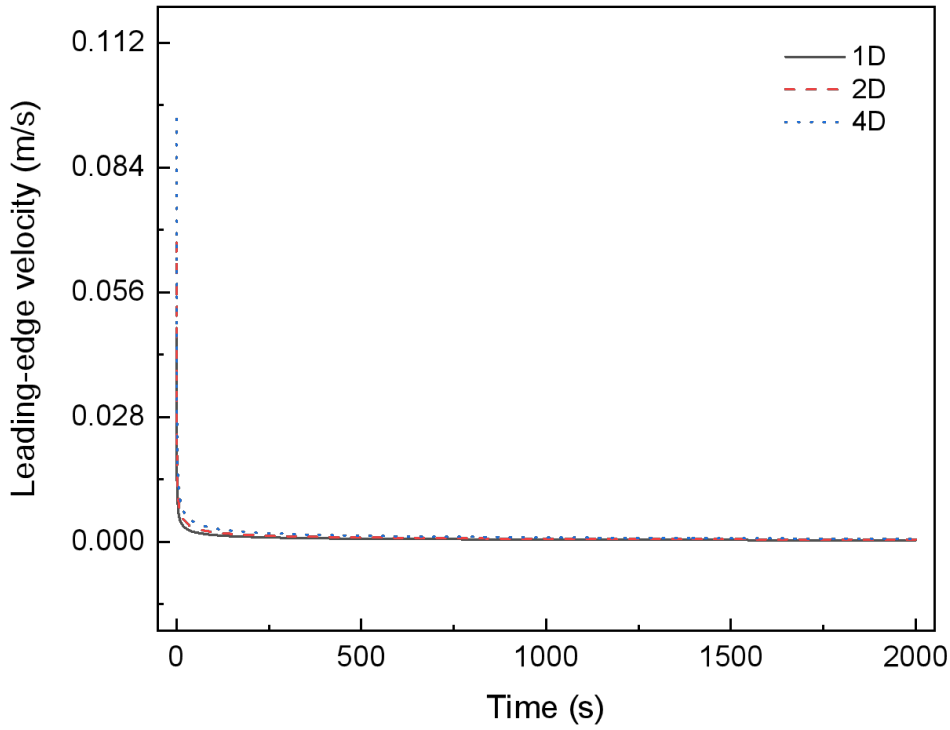

Fig. 6 Evolution of the leading-edge velocity over time under different diffusion coefficients ($D, 2D, 4D$)

(D = *const*), the saturation curves exhibit typical exponential decay characteristics. The saturation distributions at 1 month, 1 year, and 2 years share a similar shape, with differences primarily in amplitude. Diffusion is largely stabilized within 100 m after one month, highlighting the intrinsic regulatory effect of the reservoir's physical structure on fluid migration.

At the interface (x = 100 m) where the diffusion coefficient exhibits an abrupt change, the saturation distribution in the heterogeneous reservoir shows pronounced discontinuities compared to the homogeneous case. This phenomenon demonstrates how the coupling of pressure diffusion waves and reservoir heterogeneity leads to self-regulating closure via differential diffusion. Specifically, in the low-diffusion region (0–100 m), saturation exhibits rapid decay, forming a local high-pressure zone that delays fluid breakthrough. In contrast, in the high-diffusion region (100–500 m), the saturation distribution is more gradual due to rapid pressure dissipation reducing the driving gradient. This aligns with the principle that reservoirs inherently regulate fluid migration through their physical structure.

Although natural heterogeneity enhances storage efficiency, fluid migration eventually reaches a spatial limit, reflecting the self-limiting nature of the reservoir's physical mechanisms. Moreover, geological heterogeneity influences leakage pathways by altering local reservoir parameters, yet global diffusion effects continue to dominate the long-term sealing behavior. This confirms the system-level stability inherent in the reservoir's physical regulation mechanisms. By prioritizing the selection of suitable porous media (such as high-porosity sandstone), the dynamic sealing capability of the reservoir can be strategically enhanced, enabling a shift in engineering strategies from passive containment to active control.

4.1.2 Impact of high-permeability zones

Fig.8 illustrates the dual impact of high permeability zones on the CO_2 storage system by comparing fluid migration characteristics between these zones and intact reservoirs. As shown in the figure, within the high permeability zone (100–200 m), the saturation distribution exhibits a pronounced 'bulge' pattern. This anomaly arises primarily from two competing mechanisms:

(1) The rapid transport effect within the high permeability zone, which significantly enhances local migration velocity and forms preferential flow pathways;

(2) The pressure dissipation effect, where enhanced permeability accelerates pressure equilibration, thereby reducing the saturation gradient by approximately 30%–40%, and leading to the emergence of a long-term (t > 1 year) self-plugging effect.

The results in Fig.8 demonstrate that high permeability zones exert a significant influence on saturation distribution; in particular, the saturation decline rate slows within faulted regions. On one hand, high permeability zones accelerate the advancement of the migration front, potentially increasing short-term leakage risks and promoting vertical fluid escape. On the other hand, rapid pressure equilibration may facilitate the development of a favorable self-sealing effect within the confined high permeability region. Moreover, saturation levels gradually decline and stabilize over time. These findings highlight the critical importance of accounting for geological heterogeneity—particularly the influence of high permeability fault zones—when assessing fluid migration behavior in porous media. Furthermore, by strategically leveraging the dynamic characteristics of high permeability zones, it is possible to transform potential risks into storage advantages.

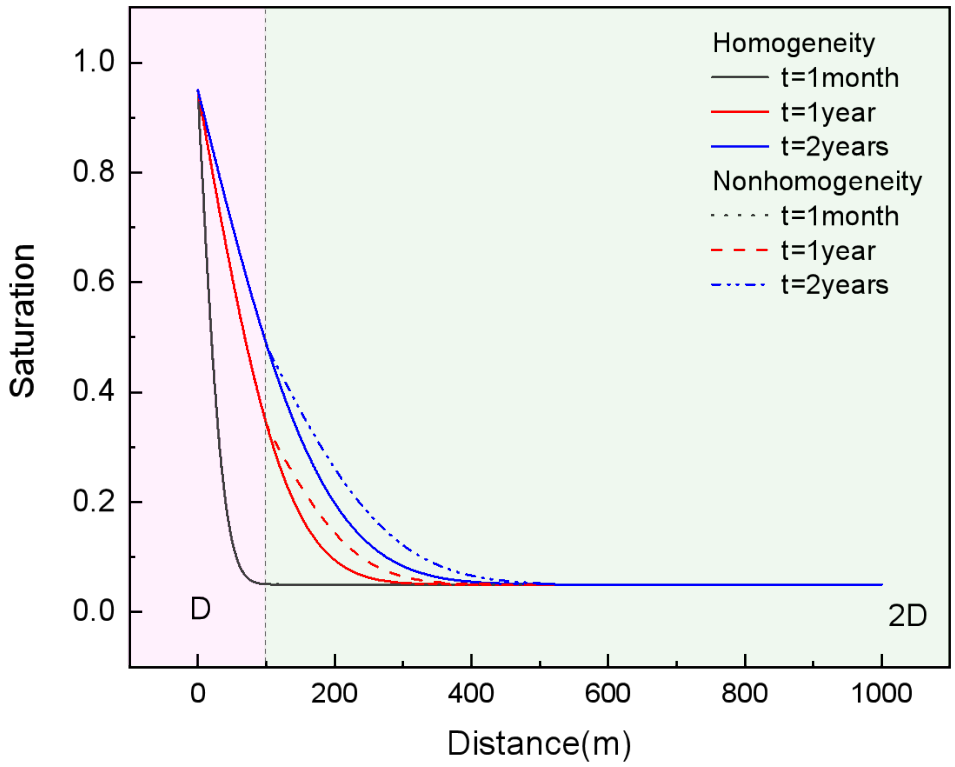

Fig. 7 Saturation Profiles Versus Distance Across Formation Interfaces (Diffusion coefficient in the 100–500 m region is twice that of the 0–100 m region)

4.2 Engineering optimization strategy and leakage risk assessment

4.2.1 Optimization of injection pressure and stepwise control

Fig.9 presents saturation profiles as a function of distance after one month of fluid migration under varying pore pressure conditions (Tab. 2). The figure clearly illustrates that variations in pore pressure significantly influence fluid migration behavior and saturation distribution. A higher initial pore pressure (2.32×10^{10}Pa) results in lower saturation, whereas a lower pressure (1.81×10^{10}Pa) yields higher saturation, consistent with findings by Bickle et al. (Bickle et al., 2007). Modeling of CO_2 migration in the subsurface reservoir of the Sleipner oilfield indicates that high-pressure injection promotes rapid CO_2 migration and plume formation, thereby reducing overall saturation. In contrast, low-pressure injection facilitates a more uniform saturation distribution.

Tab. 2 Maximum and Residual Saturation Values Corresponding to Different Injection Pressures

$P_1 - P_0$**(Pa)**	S_{im}	S_{ic}
2.32×10^{10}	0.95	0.05
2.07×10^{10}	0.95	0.15
1.81×10^{10}	0.95	0.25

Under all pressure conditions, saturation decreases rapidly with increasing distance, indicating progressive dilution of the fluid front. Saturation curves under different pressures exhibit distinct decay rates within short distances (approximately 200 meters), whereas at longer distances (greater than 200 meters), saturation stabilizes and approaches zero. This suggests that the influence of the fluid front can be neglected at sufficiently long distances, and this behavior is independent of the initial pore pressure.

The results in Fig.9 indicate that pore pressure significantly affects saturation distribution, particularly during the early stage of fluid migration. Higher initial pore pressure results in lower saturation, possibly indicating more rapid diffusion of fluids in the porous medium. These findings underscore the importance of controlling injection pressure when predicting fluid migration behavior in porous media.

Moreover, the study reveals a contradiction in high-pressure injection: although an initial high pressure ($P = 2.32 \times 10^{10}$Pa) improves the displacement efficiency, it also increases the migration range x_{leat} by approximately 30% (Fig.9). Additionally, high-pressure injection enhances pressure diffusion ($D \propto P^{0.5}$), thereby shortening the closure time t_{seal} by approximately 30%. T Therefore, a stepped injection strategy can be adopted in practical engineering: Stage 1 (t < 6 months): low-pressure injection ($P_{low} = 0.8P_{max}$) to suppress initial leakage; Stage 2 (t ≥ 6 months): high-pressure injection ($P_{high} = 1.2P_{low}$) to promote long-term diffusion balance. Moreover, the pressure threshold should be adjusted based on the reservoir diffusion coefficient (D) to ensure that the injection period t_{seal} remains within the project evaluation cycle.

Injection pressure influences leakage and sealing behavior through nonlinear coupling; the stepped strategy balances short-

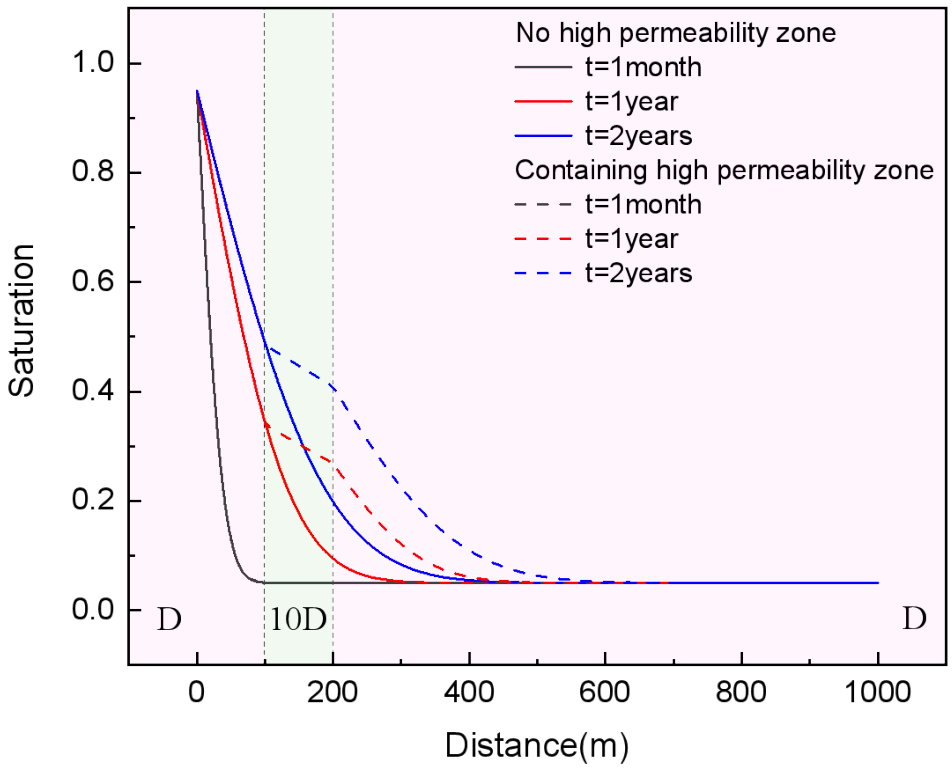

Fig. 8 Saturation distribution as a function of distance within high permeability zones

term risk with long-term stability. Furthermore, future studies should consider the coupling effect of reservoir heterogeneity and pressure regulation to establish a more accurate predictive model.

4.2.2 Leakage dynamics assessment and engineering tolerance control strategy

Based on the coupled model of pressure diffusion waves and two-phase flow, leakage behavior is primarily governed by the advance velocity of the saturation front (Eq. 13) and the attenuation of the pressure gradient (Eq. 4). When $v_f(t) \propto t^{-1/2}$ and $\nabla P \propto \mathrm{erfc}(x/\sqrt{4Dt})$, the leakage risk decays exponentially over time, resulting in a self-inhibiting closure effect. The results of this study demonstrate that the dynamic leakage process exhibits clear spatiotemporal evolution characteristics:the front propagation speed follows a power-law attenuation trend, whereas the pressure gradient decays exponentially.This coupled attenuation mechanism significantly contributes to a self-limiting migration behavior after t > 6 months,providing a physical basis for the natural suppression of leakage risk.

By employing an enhanced error function model, this study enables accurate prediction of the leakage-affected range. The theoretical model indicates that when the diffusion coefficient is 1.67×10^{-4} m^2/s, the characteristic influence ranges after 6 months and 2 years reach approximately 250 ± 10 m and 450 ± 10 m, respectively. Furthermore, the maximum potential extent of leakage can be quantitatively defined using the analytical solution (see Fig.2 and Eq. 12), offering a theoretical reference for engineering risk assessment and control threshold design.

$$x_{leak}(t) = 2\sqrt{Dt}erf^{-1}(1 - \frac{x_{leak}}{x_{max}}) \tag{14}$$

According to the ratio of the leakage front position to the predicted maximum range, the leakage risk can be classified, and appropriate control measures can be formulated. For instance, in this analysis, if $x(t) > 0.8x_{\max}$, it is classified as Level I, requiring immediate suspension and remediation. If $0.5x_{\max} < x(t) \leq 0.8x_{\max}$, it is categorized as Level II, necessitating regulation by reducing pressure. If $x(t) \leq 0.5x_{max}$, it is classified as Level III, allowing for routine monitoring. Additionally, if the reservoir monitors well spacing $L > x_{leak}(t_{\max})$, the leakage can be controlled locally.

The traditional definition of leakage is overly absolute. Leakage should not be considered a total failure; rather, it is a transient process governed by the diffusion coefficient. Its evolution exhibits time dependence, spatial self-limitation, and mass conservation. Based on these characteristics, the concept of allowable leakage $Q_{\text{leak}} = \varphi \int_0^{x_{\text{leak}}} S(x,t)dx$, should be defined, enabling a re-interpretation of traditional leakage behavior. If $Q_{leak} < 0.1\%Q_{injected}$ (the environmental capacity threshold), short-term micro-leakage can be tolerated (see Fig.3). Future research will focus on the development of dynamic risk assessment algorithms, transitioning from the ‘zero leakage’ absolute standard to a ‘risk-controllable’ dynamic standard, as well as adjusting storage technologies from passive protection to an active regulation mode.

In this section, by combining analytical solutions with engineering case studies, the dynamic sealing mechanism of leak-

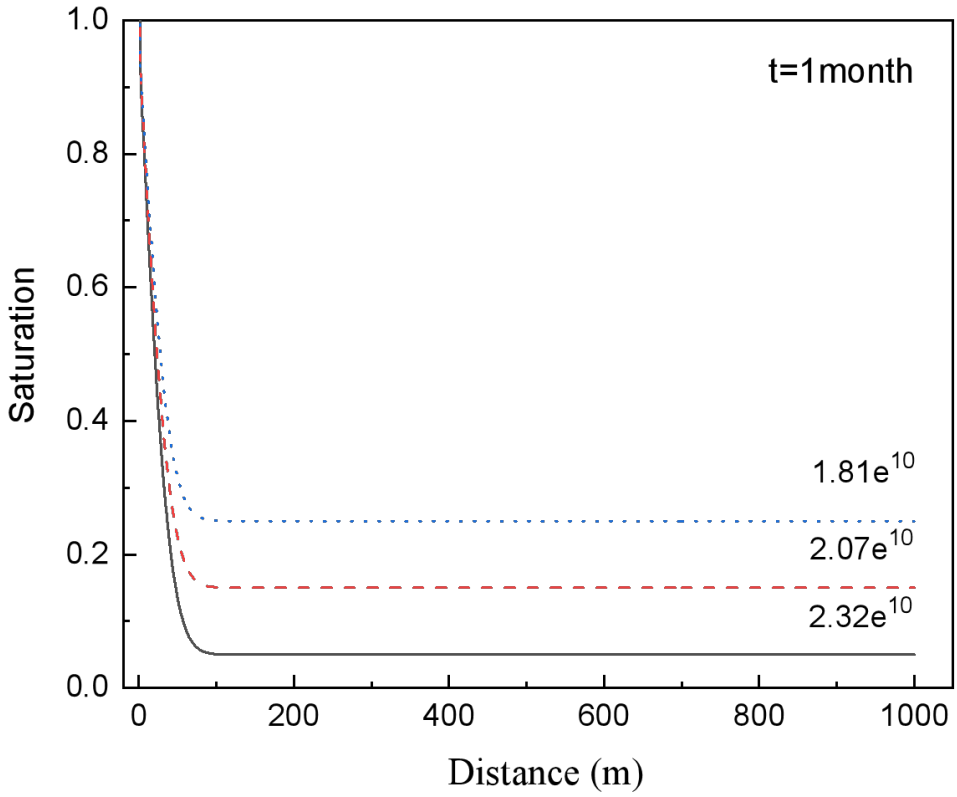

Fig. 9 Saturation variation with distance after one month of migration under different injection pressures

age, primarily governed by pressure diffusion waves, is clarified. The concept of 'acceptable leakage' and the associated hierarchical control strategies are introduced. From heterogeneous reservoir design to injection parameter optimization, this model provides a decision-making tool that integrates both physical rigor and engineering practicality for CO_2 storage engineering.

5 Conclusions

In this study, a one-dimensional coupled model of two-phase seepage and pore pressure diffusion wave–saturation interaction was developed based on pore pressure diffusion wave theory. Analytical solutions for fluid saturation distribution and the advancement of the migration front were derived. The coupling mechanisms between pore pressure diffusion waves and two-phase seepage, along with their application to CO_2 geological storage, were systematically analyzed. The key findings are summarized as follows:

(1) Theoretical model and analytical solution: By coupling the single-phase pore pressure diffusion wave model with a two-phase seepage model, an analytical solution for saturation distribution was derived. This solution effectively describes the dynamic evolution of fluid saturation in porous media, avoids numerical discretization errors, and serves as an efficient tool for parameter sensitivity analysis. The theoretical results provide a new foundation for the quantitative analysis of fluid migration in porous media.

(2) Influence of key parameters: The diffusion coefficient and permeability are key parameters influencing fluid migration. A higher diffusion coefficient promotes a more uniform distribution of fluid and reduces the advancement rate of the saturation front, while variations in pore pressure directly impact short-term migration and are governed by diffusion equilibrium in the long term. The regulatory role of these parameters is crucial for understanding and predicting long-term fluid migration behavior.

(3) Fluid migration follows a staged evolution process. In the early phase, it is primarily driven by rapid pressure propagation, whereas in later stages, it gradually stabilizes into a diffusion-dominated regime. During initial injection, the velocity of the migration front attenuates according to a power law, and the saturation profile exhibits a steep gradient. Over time, the profile flattens, and the migration rate declines. This evolutionary trend highlights the dynamic interplay between pore pressure diffusion waves and two-phase seepage.

(4) Analysis of heterogeneous reservoirs and high permeability zones indicates that differential diffusion can lead to self-regulating closure mechanisms. A stepped injection pressure strategy can effectively balance short-term leakage risk with long-term storage stability. Furthermore, a leakage risk classification framework and dynamic evaluation methodology were proposed, clarifying the concept of 'acceptable leakage' and providing a quantitative foundation for engineering monitoring and risk control.

The model developed in this study demonstrates promising applicability in both theoretical and engineering contexts. Nevertheless, for real-world applications, it is necessary to consider multidimensional and heterogeneous coupling effects that

govern CO_2 migration. In addition, interfacial phenomena such as interfacial tension and wettability exert significant control on capillary pressure and on the shape of relative permeability–saturation relationships. While these effects were neglected here to enable tractable analytical solutions, their exclusion inevitably limits the model' s completeness. Future research should therefore extend the framework to incorporate geological heterogeneity, multidimensional flow, and calibrated P_c-S_w and K_r-S_w curves, thereby improving predictive reliability and supporting the development of safer and more efficient CO_2 geological storage strategies.

Acknowledgements

This work was supported by the Key Projects of the Geology Joint Fund of the National Natural Science Foundation of China (U2344226).

Conflict of interest

The authors declare no competing interest.

References

Abanades JC, Akai M, Benson S, et al. 2005. IPCC special report on carbon dioxide capture and storage. *Cambridge University Press*.

Abdullahi MB, Jufar SR, Lee JH, et al. 2024. A coupled displacement-pressure model for elastic waves induce fluid flow in mature sandstone reservoirs. *International Journal of Rock Mechanics and Mining Sciences*. **183**, 105928. doi:10.1016/j.ijrmms.2024.105928.

Bickle M, Chadwick A, Huppert HE, et al. 2007. Modelling carbon dioxide accumulation at Sleipner: Implications for underground carbon storage. *Earth and Planetary Science Letters*, **255**(1–2): 164–176. doi:10.1016/j.epsl.2006.12.013.

Blunt MJ, Lin Q. 2022. Flow in porous media in the energy transition. *Engineering*, **14**(7): 10–14. doi: 10.1016/j.eng.2021.08.008.

Buckley SE, Leverett MC. 1942. Mechanism of fluid displacement in sands. *Transactions of the AIME*, **146**(01): 107–116. doi: 10.2118/942107-G.

DiCarlo DA. 2004. Experimental Measurements of Saturation Overshoot on Infiltration. *Water Resources Research*, **40**(4), W04215. doi:10.1029/2003WR002670.

Garcia RO, Silveira GP. 2024. Essentially Non-Oscillatory Schemes Applied to Buckley-Leverett Equation with Diffusive Term. *Latin-American Journal of Computing*, **11**: 44-54. doi:10.5281/zenodo.10402169.

Jha B, Juanes R. 2007. A locally conservative finite element framework for simulation of coupled flow and reservoir geomechanics. *Acta Geotechnica*, **2**(3): 139–153. doi:10.1007/s11440-007-0033-0.

Kenzhebek Y, Imankulov T, Bekele SD, et al. 2025. Coupled pressure and saturation prediction for two-phase flow in porous media using physics-informed neural networks (PINNs). *Computer Methods in Applied Mechanics and Engineering*, **446**(Part A), 118229. doi:10.1016/j.cma.2025.118229.

Keranen KM, Weingarten M, Abers GA, et al. 2014. Sharp increase in central Oklahoma seismicity since 2008 induced by massive wastewater injection. *Science*, **345**(6195): 448–451. doi:10.1126/science.1255802.

Kim J, Tchelepi HA, Juanes R. 2011. Stability and convergence of sequential methods for coupled flow and geomechanics: Drained and undrained splits. *Computer Methods in Applied Mechanics and Engineering*, **200**(23–24): 2094–2116. doi:10.1016/j.cma.2011.02.011.

Lei XL, Tamagawa T, Tezuka K, et al. 2011. Role of drainage conditions in deformation and fracture of porous rocks under triaxial compression in the laboratory. *Geophysical Research Letters*, **38**(24), L24310. doi:10.1029/2011GL049888.

Lei XL, Yu G, Ma S, et al. 2008. Earthquakes induced by water injection at 3 km depth within the Rongchang gas field, Chongqing, China. *Journal of Geophysical Research: Solid Earth*, **113**(B10), B10310. doi:10.1029/2008JB005604.

Leverett MC, Lewis WB. 1941. Steady flow of gas-oil-water mixtures through unconsolidated sands. *Transactions of the AIME*, **142**(01): 107–116. doi:10.2118/941107-g

Li DW, Zhang LH, Zhou KM, et al. 2008. Mechanism of gas-water two-phase flow in a visualized microscopic pore model. *Journal of China University of Petroleum (Edition of Natural Science)*, **32**(3): 80–83.

Li Q, Fei W, Liu X, et al. 2014. Numerical simulation of CO_2 geological storage in deep saline aquifers with consideration of geochemical reactions. *Greenhouse Gases: Science and Technology*, **4**(4): 452–468. doi:10.1016/j.jcp.2019.109053

Lu X, Wheeler MF. 2020. Three-way coupling of multiphase flow and poromechanics in porous media. *Journal of Computational Physics*, **401**, 109053. doi:10.1016/j.jcp.2019.109053

Mandelis A. 1991. Green's functions and mathematical methods of diffusion-wave fields. *Journal of Physics A: Mathematical and General*, **24**(11): 2485–2501. doi:10.1007/s00603-013-0531-3

Mandelis A. 2001. *Green functions and mathematical methods of diffusion-wave fields*. Springer-Verlag.

Mandelis A, Hess P. 1997. *Progress in Photothermal and Photoacoustic Science and Technology (Vol. III)*. SPIE Optical Engineering Press.

Nordbotten JM, Celia MA. 2011. *Geological storage of CO_2: Modeling approaches for large-scale simulation*. John Wiley & Sons.

Norris AN. 1993. Low-Frequency Dispersion and Attenuation in Partially Saturated Rocks. *The Journal of the Acoustical Society of America*, **94**(1): 359–370. doi:10.1121/1.407101

Nwankwo IV, Dejam M, Quillinan SA. 2025. A critical review of experimental and theoretical studies on shale geomechanical and deformation properties, fluid flow behavior, and coupled flow and geomechanics effects during production. *International Journal of Coal Geology*, **306**,104777. doi:10.1016/j.coal.2025.104777

Pruess K, Oldenburg C, Moridis G. 1999. *TOUGH2 User's Guide, Version 2.0*. Lawrence Berkeley National Laboratory. Retrieved from https://escholarship.org/uc/item/1gg7q0cm

Rasouli V, Sutherland A. 2014. Geomechanical characteristics of gas shales: A case study in the North Perth Basin. *Rock Mechanics and Rock Engineering*, **47**(6): 2031–2045. doi:10.1007/s00603-013-0531-3

Silin D, Korneev V, Goloshubin G. 2003. Pressure diffusion waves in porous media. *SEG Technical Program Expanded Abstracts 2003*: 2323-2326. doi:10.1190/1.1817821

Sminchak J, Gupta N. 2003. Aspects of induced seismic activity and deep-well sequestration of carbon dioxide. *Environmental Geosciences*, **10**(2): 81-89. doi:10.1306/eg100202009

Thomsen L. 1995. Elastic anisotropy due to aligned cracks in porous rock. *Geophysical Prospecting*, **43**(6): 805–829. doi:10.1111/j.1365-2478.1995.tb00282.x

Wang K, Liu ZC, Yang JG. 2021. Numerical Study of Gas -Liquid Two -Phase Flow in PEMFC Cathode Flow Channel with Different Diffusion Layer Surface Structure. *Journal of Power and Energy Engineering*, **9**: 106-117. doi:10.4236/jpee.2021.911006.

Wang R. 2021. Study on productivity of fractured wells for oil-water two-phase flow in low permeability reservoirs. *Oil and Gas Reservoir Evaluation and Development*, **11**(5): 760–765. doi:10.13809/j.cnki.cn32-1825/te.2021.05.014.

Yang DX, Li Q, Zhang LZ. 2015. Propagation of pore pressure diffusion waves in saturated porous media. *Journal of Applied Physics*, **117**(13), 134902. doi:10.1063/1.4916805.

Yang DX, Wang S, Zhang Y. 2014. Analysis of CO_2 migration during nanofluid-based supercritical CO_2 geological storage in saline aquifers. *Aerosol and Air Quality Research*, **14**(5): 1411-1417. doi:10.4209/aaqr.2013.09.0292.

Yang DX, Zeng RS, Zhang DL. 2011. Numerical simulation of con-

vective stability of the short-term storage of CO_2 in saline aquifers. *International Journal of Greenhouse Gas Control*, **5**(4): 986-994. doi:10.1016/j.ijggc.2010.11.004.

Yang DX, Li Q, Zhang LZ. 2016. Propagation of pore pressure diffusion waves in saturated dual-porosity media (II). *Journal of Applied Physics*, **119**(15), 154901. doi:10.1063/1.4946832.

Zhang GH, Liu XR, Li FT, et al. 2024. Experimental study on start-up pressure gradient of oil-water two-phase flow in rock cores. *Science Technology and Engineering*, **24**(13): 5372–5380. doi:10.12404/j.issn.1671-1815.2304004.

Zhang PW, Hu LM, Meegoda JN, et al. 2020. A two-phase flow model based on the 3D pore structure of geotechnical media. *Chinese Journal of Geotechnical Engineering*, **42**(1): 37–45. doi:10.11779/CJGE202001004.

Zhang YG. 2014. Full-wavefield simulation using reflectivity method in saturated fluid-porous media. *Progress in Geophysics*, **29**(3): 1369–1376. doi:10.6038/pg20140351.

Zhang Y, Ping P. 2022. Pore-pressure wave and diffusion induced by fluid-mass sources in partially saturated porous media. *Advances in Water Resources*, **164**, 104218. doi:10.1016/j.advwatres.2022.104218.